Measuring Real-World Head Orientation Priors With Naturalistic Motion Tracking in a Bayesian Multisensory Integration Framework

Lucas Billen[1]
Supervisor: Pieter Medendorp[1]

[1]*Donders Centre for Cognition, Nijmegen, The Netherlands*

Previous research has shown that the brain integrates multisensory information via Bayesian inference to achieve spatial orientation. The key feature of this approach is that, in addition to vestibular, visual, and somatosensory information, prior knowledge is incorporated in the sensory integration. The effect of such a prior is twofold: Near upright, it improves precision, but with increasing head-tilt, systematic errors in the final head-in-space estimate are induced. The prior is assumed to be based on lifelong experiences, represented as a Gaussian distribution centered on upright. Whether this accurately represents the underlying head-in-space prior was unknown. Here, we used motion tracking to kinematically measure the head orientation distributions of six participants performing naturalistic activities. We investigated whether 1) the resulting head orientation distributions can accurately represent the underlying head-in-space prior and 2) whether performances on tasks of perceived visual verticality (SVV tasks) can be simulated by incorporating the obtained real-world prior into a previously developed multisensory integration model. In line with previous research, we expected the naturalistic head orientation distributions to be best described by Gaussian distributions, accurately simulating SVV task performance. Results showed that head orientation distributions were, in fact, best fitted by t Location-Scale distributions, characterized by fatter tails compared to Gaussian distributions. Simulation of SVV task performance was not in line with previous research regarding both magnitude and direction of the biases. Thus, using a novel motion tracking approach, we provide evidence that the underlying head-in-space prior deviates considerably from normality. Future research should focus on successfully incorporating such a prior in the Bayesian multisensory integration model.

Keywords: Bayesian inference, multisensory integration, prior, motion tracking, spatial orientation, subjective visual vertical

Disclaimer: Due to regulations concerning the Covid-19 pandemic, it was not possible to collect novel data for this study, and the study had to be re-steered. This involved a novel analysis of a previously collected pilot data set of six subjects in the sensorimotor lab. Because of the limited sample size, statistical analysis lacked sufficient power.

Corresponding author: Lucas Billen; E-mail: lucas.billen@gmx.de

Spatial orientation, which is our sense of body orientation and self-motion relative to the environment, is fundamental to numerous basic motor actions, such as balance, locomotion, and the interaction with objects in the environment (MacNeilage et al., 2008). Not being able to tell how we are oriented in space could be fatal in many situations. For example, if a diver or a pilot loses their sense of spatial orientation, this could have severe consequences. However, in most situations, the brain seems to be able to achieve spatial orientation effortlessly. Given that the information from the various sensory organs is inherently noisy and partly ambiguous, how is the brain able to accurately reconstruct the state of the world and the state of the body, such that errors remain minimal?

Research has shown that the statistically optimal way of dealing with the inherent noisiness of the sensory information is to use several sources of information. The multisensory information is then integrated while their respective noisiness is taken into account in a Bayesian inference fashion (Clemens et al., 2011; De Vrijer et al., 2008; Körding & Wolpert, 2004; MacNeilage et al., 2007). According to the *Bayesian multisensory integration model* developed by Clemens and colleagues (2011) and later adapted by Alberts and colleagues (2016), the brain uses three sources of information to achieve an estimate of how the head is oriented in space (Figure 1A). Firstly, as part of the vestibular system, the otoliths directly measure acceleration of the head, and therefore provide a direct signal of how the head is oriented in space. Secondly, information from body sensors providing an estimate of the orientation of the body in space can be combined with the information provided by the neck sensors, which measure the angle between head and body. This yields a second, albeit indirect, measure of how the head is oriented in space. Thirdly, this model allows for the brain to useprior knowledge to estimate the current orientation of the head in space. This so-called *prior* is assumed to be a representation of life-long experiences of how the head is typically oriented in space (Clemens et al., 2011).

The different noisy signals are usually represented as *Gaussian probability distributions*. It is assumed that the sensory signals (i.e. information from the otoliths, and the transformed signals from the body sensors and the neck proprioceptive information) are calibrated unbiasedly, meaning that they are centered on the true head-tilt angle. However, because these signals are inherently noisy, the resulting uncertainty about the sensory information is represented in the width of the Gaussian distribution. The noisier the signal, the higher the uncertainty and therefore the broader the distribution. In terms of Bayesian inference, this means that during the integration of the sensory information, highly noisy signals are weighted less, while less noisy and therefore more reliable signals are weighted more heavily. The model assumes the noise levels of the body sensors and the neck sensors to be constant, while the noise of the sensory information coming from the otoliths increases rectilinearly with increasing head-tilt (Clemens et al., 2011; De Vrijer et al., 2008). The benefit of this Bayesian inference approach is that all of the available information is used optimally, such that the resulting head-in-space estimate has a lower degree of perceptual uncertainty than can be derived from the individual sources.

In contrast to the sensory signals, the prior is assumed to be centered around a head-tilt of zero degrees (i.e. upright), because the most likely head orientation during everyday life is assumed to be upright, too. The effect of such a prior is twofold: At small head-tilt angles, it improves precision, because it further reduces the uncertainty of the final estimate. However, the prior also induces a bias in the final estimate of head-in-space orientation, which becomes increasingly more pronounced at larger head-tilt angles (see Figure 1B). Thus, at large head-tilt angles, the prior biases the final estimate towards zero and away from the true head-tilt angle, resulting in an underestimation of one's actual head-tilt (so-called Aubert effect; Aubert, 1861; Mittelstaedt, 1983; Van Beuzekom & Van Gisbergen, 2000) (for a complete description of the model, see Methods).

These large systematic errors in one's perception of head orientation can behaviorally be measured with the so-called Subjective Visual Vertical task (SVV), hence providing a methodological approach to indirectly study the underlying multisensory integration processes taking place (Aubert, 1861; Barra et al., 2010; Ceyte et al., 2009; De Vrijer et al., 2009; Eggert, 1998; for a review on the perception of verticality, see Dieterich & Brandt, 2019). The SVV task is conducted in the dark to minimize visual influences. During the task, participants' bodies are roll-tilted while they are sitting in a vestibular chair. They are then presented with luminous bars with varying angles relative to true vertical. The participants' task is to judge whether the bar is rotated clockwise or counterclockwise compared to their perceived gravitational vertical. As was mentioned above, participants are quite accurate at this task at small head-tilt angles, but as the head-tilt increases (in some experiments up to 120°), the systematic error increases to up to

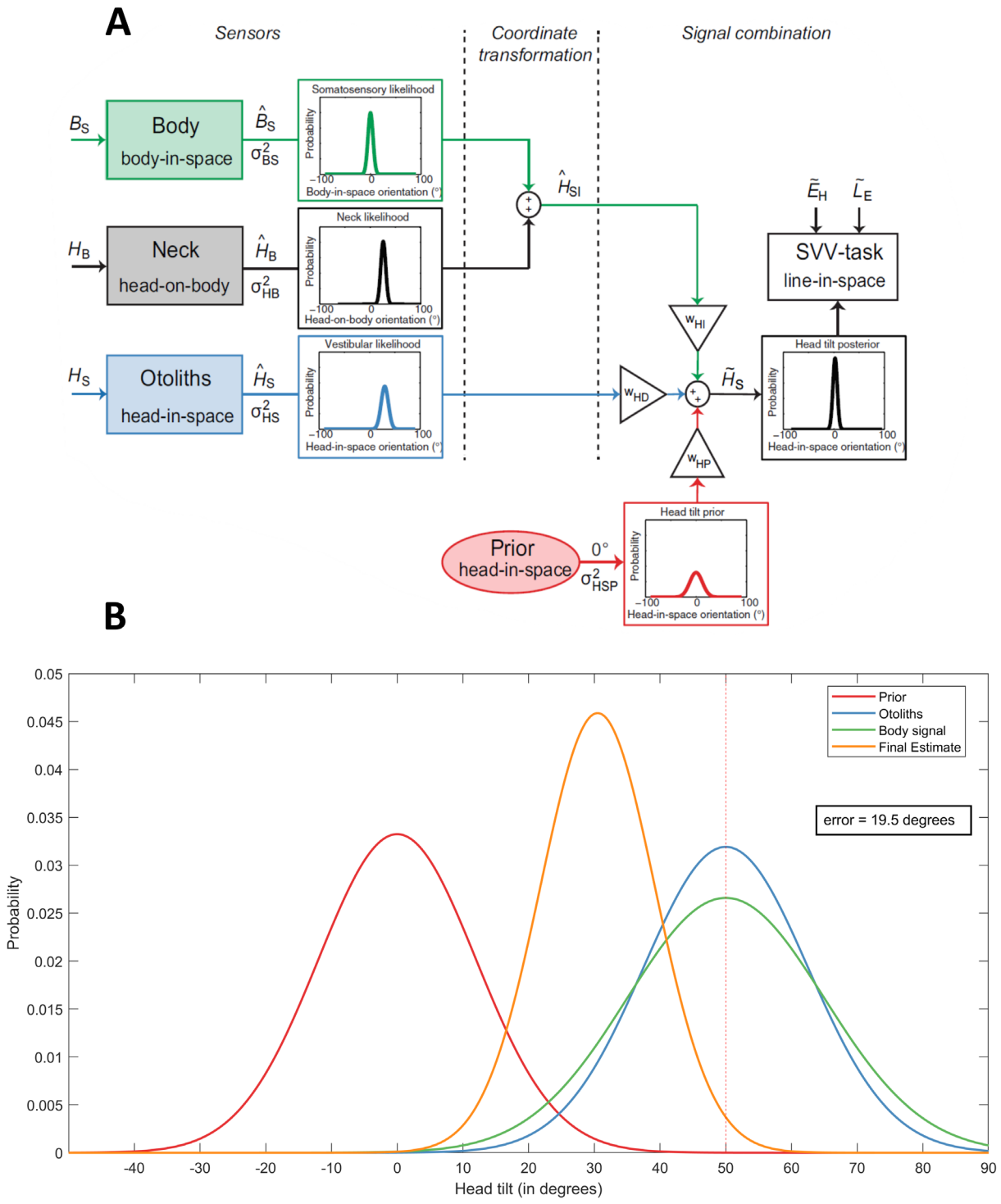

Figure 1. Bayesian multisensory integration. **A.** Bayesian multisensory integration model: The brain can use information from body sensors, neck sensors and the otoliths, represented as Gaussian probability distributions. The otoliths provide a direct measure of head-in-space orientation, while the information from the body and the neck sensors can be combined in the coordinate transformation stage to provide an additional indirect measure. Furthermore, a head-in-space prior that is centred on 0° head-tilt is assumed to be part of the signal combination stage, resulting in a final head-in-space estimate (adapted from Clemens et al. (2011) and Alberts et al. (2016)). **B.** Example of multisensory integration: The probability of the sensory estimate of head orientation in space (otolith and body sensors) can be represented as Gaussians centred on the true tilt angle (i.e. 50°) and corrupted by noise, represented by the width of the Gaussian. The Gaussian prior is centred on upright (i.e. 0°). Thus, the final estimate which is given by the optimal integration of the sensory information and the prior, will be biased toward the prior, but with smaller uncertainty with respect to the individual sources.

60° (which means that the luminous bar has to be tilted 60° to be perceived as vertical), indicating a strong underestimation of one's own head-tilt. The aforementioned multisensory integration can explain the observed behavior on this task adequately, even though performances on the SVV task can differ substantially between individuals (Clemens et al., 2011). The large systematic error can be accurately explained by the prior introducing a bias towards upright.

Even though the model provides a good fit to the data and is intuitively appealing, there is still uncertainty about the true underlying nature of the distributions of the various signals. For example, it is assumed that the prior is based on lifelong experiences of how the head is typically oriented in space. Given the observation that the head's vertical axis is usually aligned with gravity, it is justified to assume that the prior is centered on a head-tilt of 0°. However, in previous research, the prior distribution was always assumed to be Gaussian for reasons of computational convenience and/or simplicity. On the one hand, this makes the modelling easier and more intuitive. However, having a fixed distribution type makes it impossible to determine whether the model reflects the true underlying nature of the prior distribution (Stocker & Simoncelli, 2006). In other words, whether a Gaussian distribution reflects the true underlying nature of the prior, and whether potential differences in the underlying prior can explain the individual differences on SVV task performance, were not addressed in previous research regarding head orientation in space.

The present study aimed to tackle these questions. Because it is assumed that the prior is based on lifelong experiences, *naturalistic motion tracking* might be a viable approach to measure the underlying prior. Thus, we used motion tracking to measure kinematic head movements during typical naturalistic activities. Subsequently, we investigated what type of distribution fits the measured data best in an attempt to test the basic assumption that the prior is of Gaussian nature. We then used the best fitting distributions as representations of the underlying prior, by implementing them in the Bayesian sensory integration model of Clemens et al. (2011). We were able to simulate what the SVV task performance would look like in the same participants, providing us with a novel approach to gain insights into the true underlying distribution of the head-in-space prior. Thus, the current study combined a naturalistic motion tracking approach with a controlled lab-based task of perceived verticality to get a more realistic and complete view of what the underlying head-in-space prior might look like, and how it can bias perception on tasks of perceived verticality.

Not many studies have used motion tracking to investigate head movements during everyday life activities. Carriot and colleagues were the first to study the natural vestibular inputs that the brain needs to process during naturalistic activities (Carriot et al., 2014). Using a micro-electromechanical systems module, which combines three linear accelerometers and three gyroscopes, they measured participant's head movements during several active and passive movements, such as walking, running, jumping, and riding on a bus. Interestingly, they showed that the probability distributions of the angular velocities that the vestibular system experiences in everyday life also deviate significantly from normality. Instead, the probability distributions were characterized by large excess kurtoses (i.e. fatter tails). Using a similar methodological approach, while focusing more on the head-in-space orientation might therefore be a good approach to quantify naturalistic head orientations. The general study design of Carriot et al.'s study therefore serves as a good basis for the present study. Thus, similar to the study by Carriot and colleagues, participants in this study performed five naturalistic activities: walking, running, going up and down the stairs, standing and sitting. These tasks cover a wide range of activities that predominantly occur in everyday life, therefore providing a relatively realistic representation of activities that the underlying head-in-space might be based on.

In line with the Bayesian sensory integration model developed by Clemens and colleagues (2011), we expected to show that the resulting naturalistic head-in-space distributions measured by the motion trackers will be best captured by Gaussian distributions centered on 0° degrees head-tilt. Furthermore, we expected that upon implementation of those naturalistic priors into the model, a simulation of SVV task performances would closely follow the actual performances observed in past studies.

Materials and Methods

Participants

Six healthy subjects participated in the study (three male and three female). Ages ranged from 23 to 28 yrs (M = 25.5; SD = 1.64 yrs). They were free of any known neurological or movement disordershad normal or corrected-to-normal vision

and were personally recruited by the experimenter. All participants took part voluntarily and gave written consent after they were informed about the experimental procedure.

Naturalistic Motion Tracking

Experimental setup. To acquire naturalistic motion kinematics, the MVN motion capture suit from Xsens was used (Xsens, 2017). This system consists of 17 sensors for full body motion tracking. For the purpose of this project, only 11 sensors were used to measure upper body and head kinematics. Sensors were placed on the pelvis, shoulders, sternum, upper arms, forearms, hands, and head. The sensors on the torso were attached with a tight-fitting vest, the sensor on the head was attached with a headband and the sensors on the arms were attached with Velcro-straps. This equipment was provided by Xsens and therefore was designed to securely contain the sensors with integrated Velcro pockets. Each sensor is a compact Inertial-Magnetic Measurement Unit (IMMU) (47mm ×30 mm × 13mm, weight: 16 g), containing inertial sensor components, including a 3D rate gyroscope measuring angular velocities and a 3D accelerometer measuring acceleration. Additionally, it comprises a 3D magnetometer, a barometer, and a thermometer. Combined with the internal Xsens signal processing algorithms, 3D drift-free orientation data is provided. The sensors are wirelessly connected to the Awinda Station, which serves as the interface between the laptop running the Xsens-based software (MVN Analyze/Animate) and the IMMUs.

The integrated MVN Fusion Engine calculates the position, orientation, and numerous other kinematic measures of each body segment with respect to an earth-fixed reference coordinate system. By default, the earth-fixed reference is defined as a right-handed Cartesian coordinate system with X being positive when pointing to the local magnetic North, Y being oriented according to the right-handed coordinates (pointing West), and Z being positive when pointing up (Figure 2A).

For each body segment, all kinematic quantities are expressed in a common, local coordinate frame, L, which is also a right-handed coordinate system with X being positive when pointing forward, lying in the horizontal plane, Y being oriented according to the right-handed coordinate system with respect

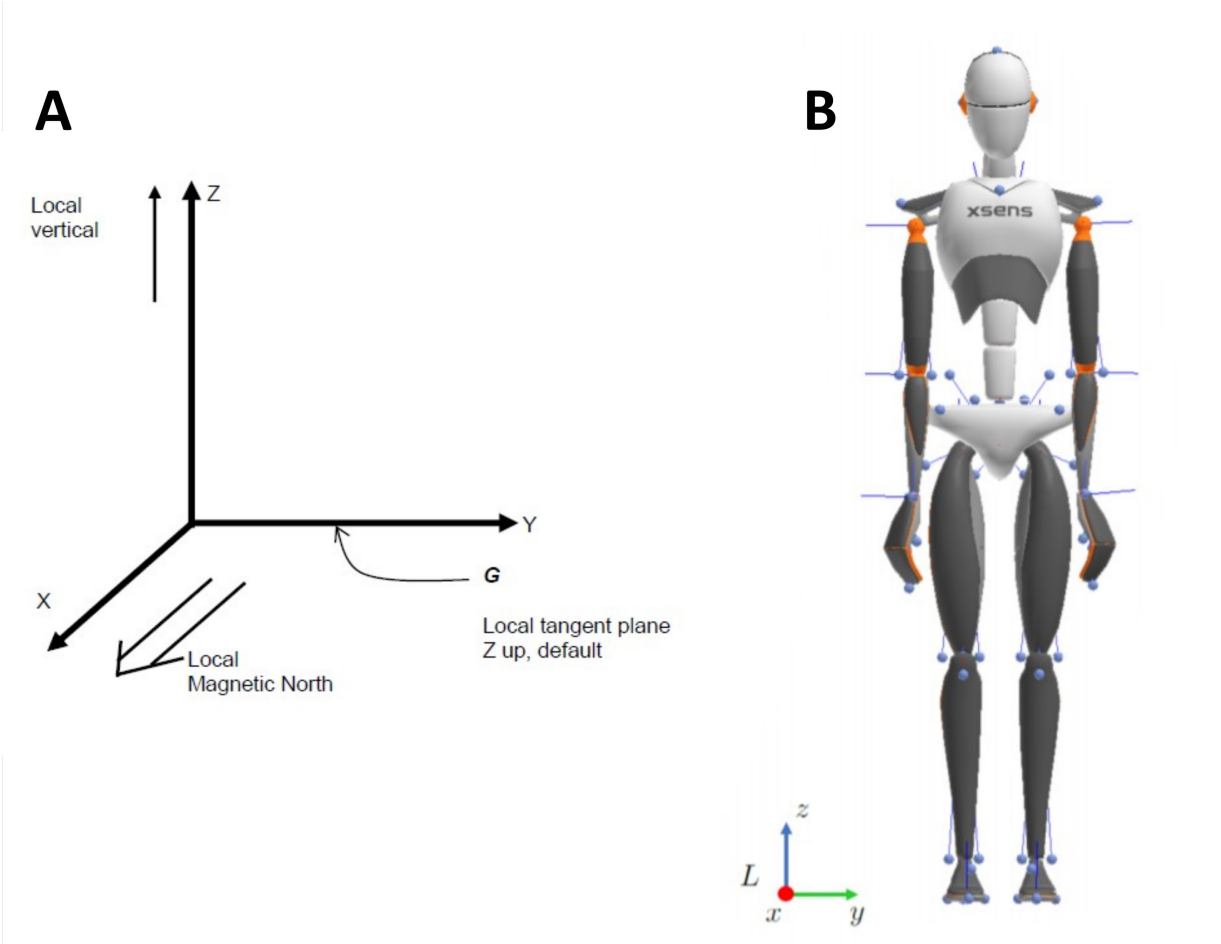

Figure 2. Global and local reference frames. **A.** Representation of the earth-fixed reference coordinate system. **B.** MVN avatar in N-pose.

to X and Z, and Z being positive when pointing upwards along the vertical, gravity referenced, axis. The system was calibrated while the participant was standing in a neutral position ('N-pose'), as shown in Figure 2B. In this pose, the participant is standing in a relaxed, upright position, with the feet being parallel to each other and the arms flat against the body, while looking straight ahead with a natural head position.

Procedure. During the experiment, participants were asked to perform five different tasks, namely walking, running, going up and down the stairs, sitting and standing. The walking and running tasks were performed outside on a standard sidewalk on campus. Going up and down the stairs was done in the university building and the sitting/standing task was performed on a normal office chair in the lab. The first three tasks were adapted from the experiment conducted by Carriot et al. (2014). Each task was repeated three times and each repetition lasted about two minutes, resulting in roughly six minutes of recorded data for each task. The participants were instructed to perform each task at a comfortable speed and while moving and looking around as naturally as possible.

Data Analysis

Pre-Processing. The MVN software saves the orientation data of the motion-trackers in quaternion form. For the purpose of this project, the quaternion data was converted to Euler angles, because we needed to represent the head-in-space prior as a distribution comprised of angles in degrees in the roll-tilt dimension. Therefore, after importing the raw data into MATLAB (version 2019a), the orientation data of the MVN sensor that was attached to the head was converted to Euler angles represented in radians, such that

$$\varphi = atan2\left(2(q_0q_1 + q_2q_3), 1 - 2(q_1^2 + q_2^2)\right) \quad (1)$$

$$\theta = asin\left(2(q_0q_2 - q_3q_1)\right) \quad (2)$$

$$\psi = atan2\left(2(q_0q_3 + q_1q_2), 1 - 2(q_2^2 + q_3^2)\right) \quad (3)$$

in which φ equals the roll-tilt angle, θ equals the pitch angle and equals the yaw angle. q_0, q_1, q_2 and q_3 stand for the four elements that a quaternion is comprised of (Hemingway & O'Reilly, 2018). After the conversion, the data was cleaned by deleting outliers that deviated more than four standard deviations from the mean. Lastly, the data was converted from radians to degrees.

Distribution fitting. We characterized the data based on their four statistical moments, namely the mean, the variance, the skewness, and the kurtosis. Shortly, in probability and statistics, the mean or expected value is a measure of the central tendency of a probability distribution, i.e. the location of the distribution. The second moment, the variance, provides information about the spread of the distribution. The third moment, the skewness, is a measure of the asymmetry of a probability distribution. A normal distribution (or any other symmetrical distribution) has a skewness of zero. A negative skew indicates that the left tail of the distribution is longer, and a positive skew indicates that the right tail is longer. Lastly, the kurtosis is a measure regarding the tails of a distribution. A normal distribution has a kurtosis of three. A kurtosis greater than three (i.e. excess kurtosis), indicates that the probability distribution has fatter tails, which means that it produces more outliers. Additionally, the peak of the distribution is oftentimes higher and sharper (Brown, 2016). Just like the skewness, the kurtosis is a measure of the shape of the distribution.

To test which distribution type best represents the measured head orientation data and therefore the underlying head-in-space prior, multiple distributions were fitted to the converted roll-tilt data of the MVN sensor. The fitting procedure was performed via the opensource function 'fitmethis' (De Castro, 2020). This function finds the distribution that best fits the data among all distributions available in MATLAB's built-in Maximum Likelihood Estimation function (for a complete overview of the fitted distributions and their respective parameters, see Appendix). Because some distributions can only be fitted to non-negative data (such as the Weibull distribution), we added a constant of 100 degrees to the head orientation data, so that the distributions are roughly centered on 100 degrees head-tilt (instead of 0). This did not affect the actual fitting procedure. The distributions are then ranked according to their Log-Likelihood. This procedure provided us with the necessary distribution-specific parameters which we subsequently used to represent the underlying head-in-space prior. It should be noted that we would formally have to fit circular distributions, because we are dealing with rotation data (De Winkel et al., 2018; Murray & Morgenstern, 2010). However, because the standard deviations of the head orientation data were rather small, differences

between the distributions that were fitted here and circular distributions such as the Von Mises distribution would be negligible (De Winkel et al., 2018). For reasons of computational simplicity, we therefore chose to fit non-circular distributions.

From the resulting fits, it became clear that the normal distribution, the (log)logistic distribution and the t Location-Scale distribution provide the best fits. These three distributions are therefore briefly introduced here.

Normal Distribution. A normal (or Gaussian) distribution is a continuous probability distribution for a real-valued random variable. The parameter μ is the mean of the distribution and σ is its standard deviation, with variance σ^2. The general form of its probability density function is

$$y = \frac{1}{\sigma\sqrt{2\pi}} e^{-\frac{1}{2}\frac{(x-\mu)^2}{\sigma^2}} \quad (4)$$

During the MLE fitting procedure, the maximum likelihood estimators of μ and σ, respectively, are

$$\bar{x} = \sum_{i=1}^{n} \frac{x_i}{n} \quad (5)$$

$$s^2_{MLE} = \frac{1}{n}\sum_{i=1}^{n}(x_i - \bar{x})^2 \quad (6)$$

where (5) is the sample mean, an unbiased estimator of the parameter μ, and (6) is a biased estimator of the parameter σ^2 (*MathWorks - Normal Distribution*, 2020). As was mentioned above, a normal distribution has, by definition, a kurtosis of 3 and is non-skewed.

Logistic Distribution. The logistic distribution is typically used for growth models and in logistic regression. It resembles the normal distribution, but it has longer tails and therefore a higher kurtosis. Its probability density function is defined as

$$f(x;\mu,\sigma) = \frac{e^{-\frac{x-\mu}{\sigma}}}{\sigma\left(1+e^{-\frac{x-\mu}{2\sigma}}\right)^2} \quad (7)$$

where μ is the mean of the distribution and σ is the scale parameter.

t Location-Scale Distribution. The t Location-Scale distribution is a generalized form of the Student's t distribution. It typically has heavier tails than the both the normal distribution and the logistic distribution. Its probability density function is given by

$$p(x\,|\nu,\mu,\sigma) = \frac{\Gamma\left(\frac{\nu+1}{2}\right)}{\Gamma\left(\frac{\nu}{2}\right)\sqrt{\pi\nu}\sigma}\left(1+\frac{1}{\nu}\left(\frac{x-\mu}{\sigma}\right)^2\right)^{-\frac{\nu+1}{2}} \quad (8)$$

where Γ**(•)** is the gamma function, μ is the location parameter, σ is the scale parameter and ν is the shape parameter. Compared to the standard Student's t distribution, which only has one parameter, ν, the t Location-Scale distribution is more flexible, because here, the scale parameter σ is independent of the shape parameter ν, which is not the case in the traditional Student's t distribution. As ν increases towards infinity, the distribution approaches the normal distribution.

Bayesian sensory integration model. Figure 1A represents the Bayesian sensory integration model that was used to implement the measured head-in-space orientation to predict the performance on the SVV task. This framework was originally developed by Clemens et al. (2011), although this version of the model is mostly based on the work by Alberts et al. (2016). The model contains three stages of information processing: an input stage, a coordinate transformation stage, and a sensory integration stage.

Sensory input. In the sensory input stage, physical information about the world is transformed to sensory signals, denoted with a hat symbol (^). It is assumed that all sensory signals are unbiased but corrupted by Gaussian noise with variance σ^2. Firstly, the otoliths provide the brain with direct information about the orientation of the head in space ($\hat{H}_S$). At small head-tilt angles this information is very precise. However, due to the physiological properties of the otoliths, it can be assumed that the noise level of the sensory information increases rectilinearly with increasing head-tilt (De Vrijer et al., 2008; Tarnutzer et al., 2009, 2010):

$$\sigma_{HS} = \alpha_{HS} * |H_S| + \beta_{HS} \quad (9)$$

Here, β_{HS} reflects the noise level of the otoliths at 0° head-tilt and α_{HS} reflects the proportional noise increase with increasing head-tilt. Secondly, neck sensors provide proprioceptive head-on-body information ($\hat{H}_B$) and thirdly, body somato-sensors respond to the orientation of the body in space ($\hat{B}_S$).

Coordinate transformation. In addition to the direct head-in-space information from the otoliths, the brain can use the information from the body somatosensors and the neck sensors to get an *indirect* measure of head-in-space orientation ($\hat{H}_{SI}$). In order to do so, the information from these two sources needs to be combined. This involves a coordinate transformation, such that

$$\hat{H}_{SI} = \hat{B}_S + \hat{H}_B \quad (10)$$

This means that the Gaussian distributions of the single sources that are centered on B_S and H_B are now combined to one Gaussian distribution centered on $B_S + H_B$.

Sensory integration. At this stage, all available information is statistically optimally combined to a single final head-in-space estimate. As was mentioned before, it is also assumed that, in addition to the sensory information, the brain uses prior information about head orientation in space. In previous research, this prior was represented as a Gaussian distribution that was centered on 0, while the variance of the prior was one of the free parameters. As was described before, we based our head-on-space prior on the motion tracking data, meaning that it is not fitted as a free parameter. This prior is denoted as H_{prior}. When integrating the sensory signals and the prior, the peak of the resulting distribution representing the head-in-space orientation estimation (the posterior) follows from Bayes' rule, and is given by:

$$\tilde{H}_S = w_{HD} * \hat{H}_S + w_{HI} * \hat{H}_{SI} + w_{HP} * H_{Prior} \quad (11)$$

with

$$w_{HD} = \frac{1/\sigma_{HS}^2}{1/\sigma_{HS}^2 + 1/(\sigma_{HB}^2 + \sigma_{BS}^2) + 1/\sigma_{Prior}^2} \quad (12)$$

$$w_{HI} = \frac{1/(\sigma_{HB}^2 + \sigma_{BS}^2)}{1/\sigma_{HS}^2 + 1/(\sigma_{HB}^2 + \sigma_{BS}^2) + 1/\sigma_{Prior}^2} \quad (13)$$

$$w_{HP} = \frac{1/\sigma_{Prior}^2}{1/\sigma_{HS}^2 + 1/(\sigma_{HB}^2 + \sigma_{BS}^2) + 1/\sigma_{Prior}^2} \quad (14)$$

Here, w_{HD}, w_{HI} and w_{HP}, are the noise-dependent weights of the direct, indirect, and prior information pathway.

Finally, the brain needs to compute the orientation of the luminous line in space. This is achieved by combining the head-in-space information ($\tilde{H}_S$) with eye-in-head information $\tilde{E}_H$ and line-relative-to-eye information ($\tilde{L}_E$). The line-relative-to-eye information itself is assumed to be unbiased, and therefore does not contribute to the resulting error. Regarding the eye-in-head information, it is assumed that the eyes automatically counter-rotate to compensate for small head-tilt angles (i.e. if the head is slightly tilted CW, the eyes rotate CCW).

However, evidence suggests that the brain does not seem to compensate for this counter-rotation, resulting in small errors in the direction opposite of the actual head-tilt at small head-tilt angles (E-effect; Palla et al., 2006). This uncompensated ocular counterroll can be represented as:

$$\tilde{E}_H = -A_{OCR} * sin(\hat{H}_S) \quad (15)$$

The final systematic error that occurs at different degrees of head-tilt angles (E-effect at small angles, A-effect at large angles) can, thus, be described as:

$$\mu(Error) = (H_S - \tilde{H}_S) + \tilde{E}_H \quad (16)$$

After having established the type of distribution that best fits the head orientation data, we forward simulated what the SVV task data might look like in these subjects, based on the multisensory integration model. We used both average values for the various parameters from previous research (Clemens et al., 2011) and, for the signal of the prior, the parameters that resulted from the distribution fitting. More specifically, we used the values from Clemens et al. (2011) for the parameters of the otolith signal, the body-in-space signal, the head-on-body signal and the ocular counterroll (α_{HS}, β_{HS}, σ^2_{BS}, σ^2_{HB}, A_{OCR}) (for an overview of the specific parameters, including the parameters for the prior signal, see Table 4 and 5). Upon simulating the SVV task data with the multisensory integration model using the best fitting distributions as the prior, we expected to find that the predicted SVV task performance between head-tilts of ±120° would closely match previously observed SVV task behavior.

Results

In the following, the shape of the different head orientation distributions and the best fitting distribution types will be discussed. This will be done by investigating the four statistical moments of a distribution. Figure 3 shows a histogram of the roll-tilt data of the head of one example subject (S4) during all five activities (44 bins). The bottom

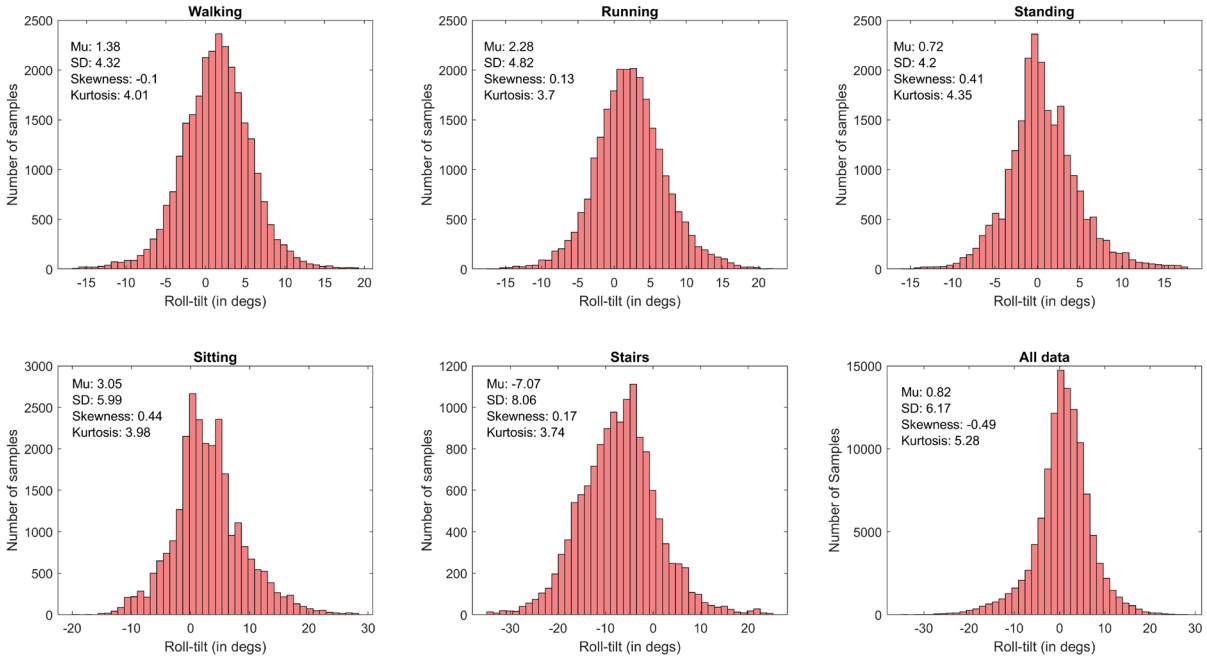

Figure 3. Example data of one subject. The number of samples of the MVN sensors is plotted as a function of roll-tilt of the head. All activities are displayed. The last subplot contains the pooled activities.

right subplot demonstrates a histogram of the data pooled across all activities. Most distributions are roughly centered on 0° head-tilt, while being relatively non-skewed. This indicates that this particular subject tends to hold their head relatively stable in the roll-dimension (i.e. with low variance) without having a bias to either the right or the left roll-tilt side. The standard deviation of the roll-tilt is lowest in the "standing" condition, which is unsurprising. Going up and down the stairs resulted in the highest variance in the roll-tilt dimension, which can potentially be explained by both the frequent gaze shifts that are necessary and by the constant shifts of the body weight when going up and down the stairs. The kurtosis of the last plot (the data of the pooled activities) is equal to 5.28 (see Table 1), indicating that this particular subject has more extreme values in the roll-tilt dimension and a higher peak than would be assumed if the distribution was normally distributed. This pattern is consistent across most subjects (Table 1).

Figure 4 shows the pooled data across all activities for each subject separately. Table1shows the four statistical moments of that data.

1. Mean: In all six subjects, the mean roll-tilt angle of the head across all activities was roughly centered on zero. Subject 1 showed the largest bias (M = -2.62 degrees). One-sample Wilcoxon signed-rank tests indicated that the median of the head orientation distributions of all subjects deviated significantly from 0° head-tilt (p< .001). However, effect sizes were rather small (effect size formula based on Rosenthal (1994); r = .25; r = .17; r = .14; r = .19; r = .20; r = .02, for S1 to S6 respectively), suggesting that the significant results are caused by the large sample sizes (≈120.000 samples per subject). Thus, on average, the participants kept their head upright, without demonstrating considerable biases to either the left or the right roll-tilt side.

2. Standard deviation: Overall, the standard deviations can be considered relatively low. It was highest for Subject 1 (SD = 9.60 degrees) and lowest for Subject 4 (SD = 6.17 degrees), meaning that the majority of the head tilts in the roll dimension were small. Overall, Subject 6 showed the most extreme head-tilts with values up to 59.6 degrees and Subject 3 had the least extreme head-tilts (33.9 degrees).

3. Skewness: The distributions from five out of six subjects were practically non-skewed, with only slight deviations from zero. Subject 2 showed

Table 1. Four statistical moments of pooled activities across subjects.

Subject	Mean	Std	Skew	Kurtosis
S1	-2.62	9.60	-0.85	5.86
S2	-1.98	7.59	-1.04	4.44
S3	0.48	6.44	-0.60	5.29
S4	0.82	6.17	-0.49	5.28
S5	1.16	6.98	0.24	6.32
S6	-0.08	6.26	0.12	5.87

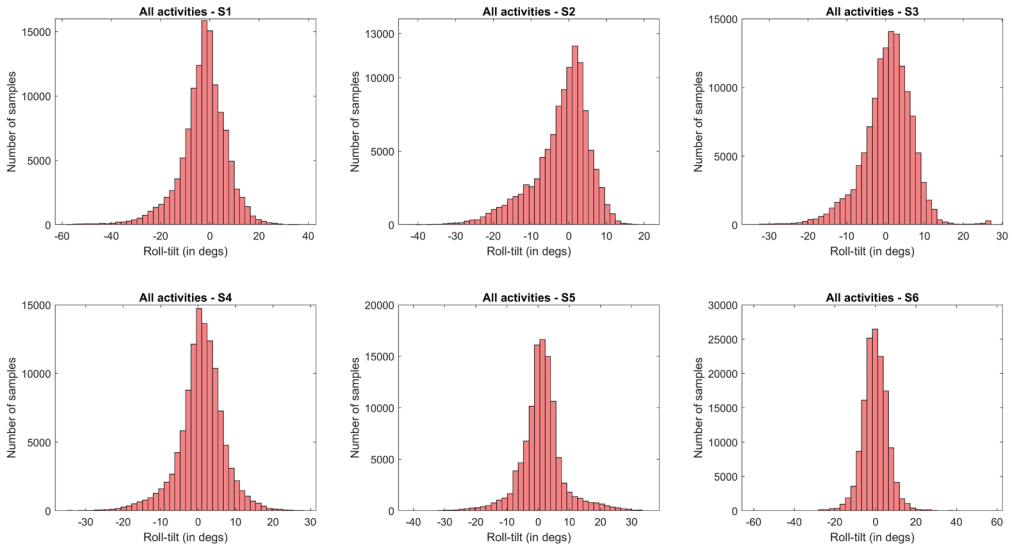

Figure 4. All pooled activities across subjects. *Note.* S = Subject.

Table 2. Best-fitting distributions and their respective log-likelihoods. *Note.* Note that not the absolute values should be interpreted, but the value relative to the other fits. The higher the value, the better the fit (relative to the others).

Subject	Best fits	Log-Likelihood
S1	t Location-Scale distribution	-442350.66
	Logistic distribution	-443412.15
	Loglogistic distribution	-447007.89
	Weibull distribution	-447266.82
S2	Extreme Value distribution	-367709.04
	Weibull distribution	-367739.56
	t Location-Scale distribution	-373448.99
	Logistic distribution	-373756.24
S3	t Location-Scale distribution	-432454.20
	Logistic distribution	-432981.81
	Loglogistic distribution	-434876.83
	Normal distribution	-437678.17
S4	t Location-Scale distribution	-369039.59
	Logistic distribution	-369984.30
	Loglogistic distribution	-371200.89
	Normal distribution	-374895.08
S5	t Location-Scale distribution	-349880.51
	Logistic distribution	-354003.98
	Loglogistic distribution	-354033.10
	Nakagami distribution	-361908.37
S6	t Location-Scale distribution	-454105.05
	Logistic distribution	-454405.78
	Loglogistic distribution	-454651.04
	Normal distribution	-458572.73

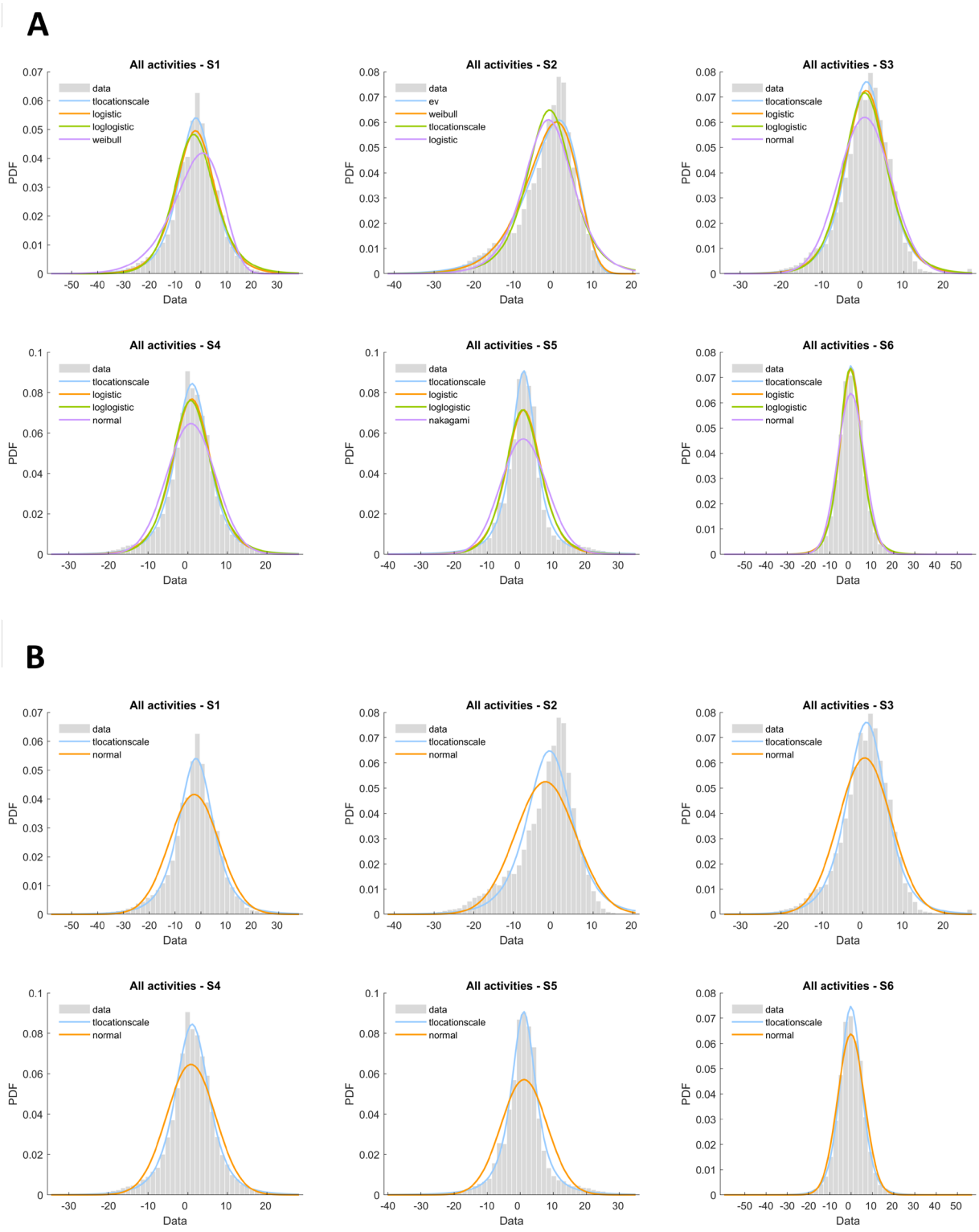

Figure 5. Distribution fitting. S = Subject; PDF = probability density function. **A.** The four best-fitting distribution types for each individual are shown, plotted on top of the data. Distributions can, thus, differ between individuals. Distributions are sorted by best fit (blue = best fit; orange = second-best fit etc.). **B.** Fitted normal distributions vs. t Location-Scale distributions plotted on top of the data for each individual.

the largest asymmetry (-1.04), which is also visible in Figure 4. As a general rule of thumb, skewness values that exceed ±1 can be considered highly skewed (*Normality Testing - Skewness and Kurtosis*, n.d.).

4. Kurtosis: The distributions of all subjects showed excess kurtoses (>3), with values ranging from 4.44 (S2) to 6.32 (S5), which indicates that there were more outliers (i.e. fatter tails) and higher peaks than would be expected if the data were normally distributed.

Summarizing, for all subjects the head orientation distributions were all roughly centered on 0° roll-tilt, with relatively small standard deviations, supporting the assumption that the prior is centered on upright. Furthermore, the distributions of five out of six subjects were practically symmetrical. Only subject 2 demonstrated a considerable skewness of the head orientation data to the left. Notably, all subjects had head orientation distributions with excess kurtosis, which deviate considerably from what would be expected under the assumption that the data are normally distributed.

Distribution fitting

Figure 5A shows the four best fitting distributions, superimposed on the combined roll-tilt head orientation data of all subjects. Table 2 shows the corresponding log-likelihoods for those fits. It should be noted that, in theory, the log-likelihood can lie between and and the values in itself are not meaningful. The values can only be compared to other log-likelihoods. The results show that in five out of six cases, the t Location-Scale distribution provided the best fit to the data, as indicated by the highest log-likelihoods. For subject 2, the extreme value distribution provided the best fit. This is presumably caused by the fact that this head orientation distribution is the most asymmetric one, therefore resulting in worse fits of distributions that are by definition symmetric, such as the normal distribution or the t Location-Scale distribution.

Importantly, the Gaussian distribution does not fit the data well. Figure 5B shows a comparison between the fits of the t Location-Scale distribution and the normal distribution. In contrast to the fit of the normal distribution, the t Location-Scale distribution follows the data much more closely, providing a better representation of the data and, consequently, a more realistic depiction of what the underlying head-in-space prior might look like. Most strikingly, the normal distributions are not able to follow the fat tails of the data, which in turn results in lower-than-optimal peaks. This means that they underrepresent the amount of the head-tilt data that lies closely around 0°. Hence it follows that the spread of the normal distributions around the inflection points is too large, resulting in an overestimated spread of the data. Furthermore, the excess kurtoses of the data, and therefore its 'tailedness', cannot be captured by the normal distributions, because, by definition, they have a kurtosis of three. It seems logical that the tLocation-Scale distribution provides a better fit compared to the Gaussian distribution, because it has one parameter more that can be flexibly fitted to the data. Therefore, to avoid overfitting, we additionally compared the distribution fits based on the Akaike Information Criterion (AIC).The AIC deals with the risk of over fitting by punishing an increasing number of parameters, therefore providing a more objective measure when comparing models with different numbers of parameters. Generally, a difference in AIC scores of more than 10 means that there is essentially no empirical support for the

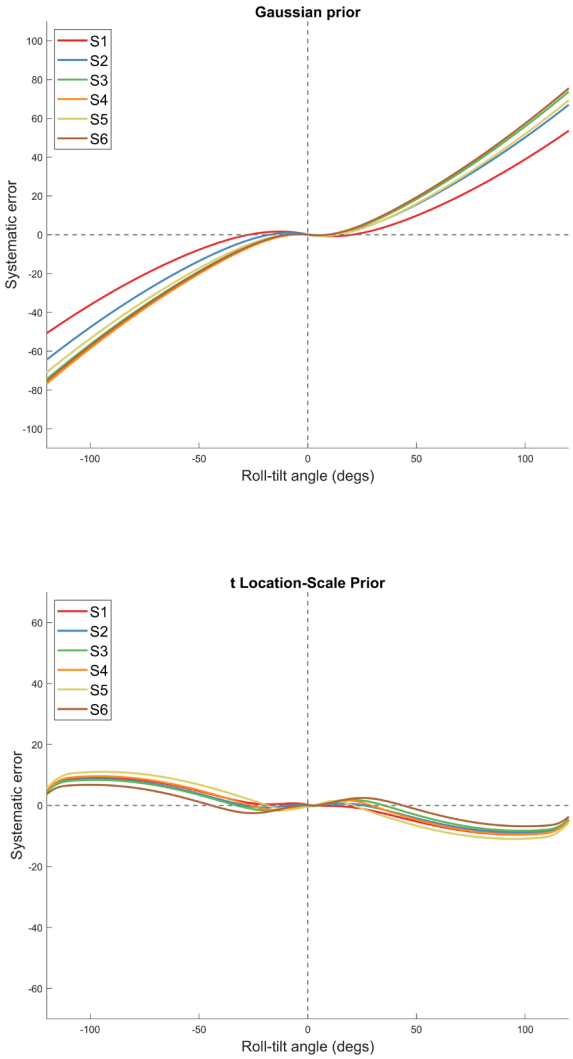

Figure 6. Model simulation of the systematic errors for all subjects. *Note.* S = Subject.

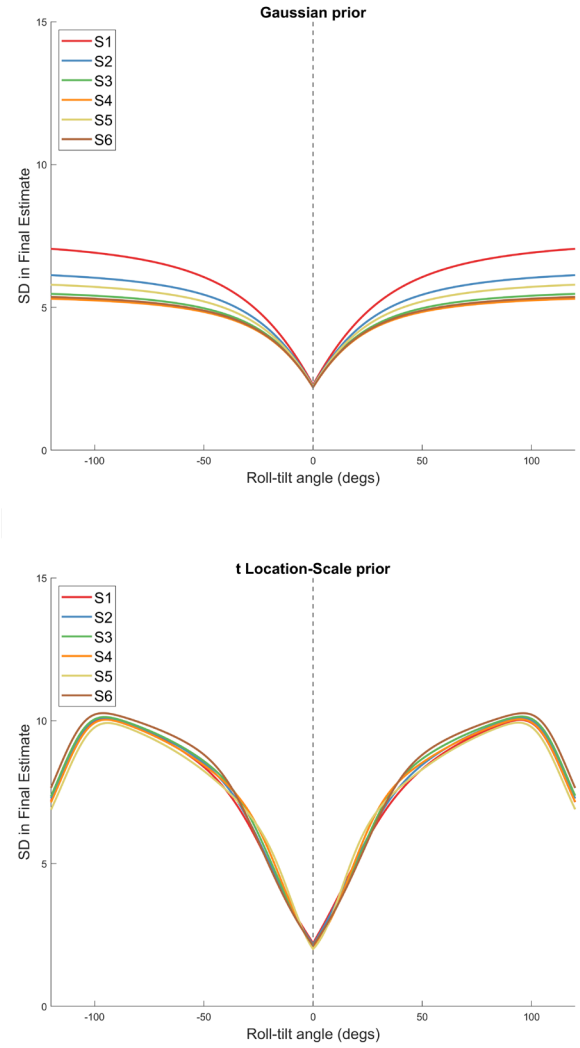

Figure 7. Model simulation of the standard deviations of the final head-in-space estimate. *Note.* S = Subject.

model with the higher AIC (Burnham & Anderson, 2002; Cavanaugh & Neath, 2019). Thus, the smaller the AIC score, the better the fit of the distribution (relative to the other distribution fits). As can be inferred from Table 3, the AIC scores for the t Location-Scale distribution fits are substantially smaller than the AIC scores for the Gaussian distribution, providing further evidence that the t Location-Scale distribution provide a significantly better fit compared to the Gaussian distributions.

To summarize, the normal distributions do not provide a good fit for the naturalistic head orientation data. The data is more peaked and has fatter tails than what a normal distribution is able to capture. Instead, the t Location-Scale distribution provides both the best overall fit in five out of the six subjects and in all six cases a better fit than the normal distribution. Due to its three parameters (location, scale and shape parameter), it is more flexible and therefore better suited to capture this particular dataset and, consequently, mightbe a better representation of the underlying head-in-space prior.

Model Simulation

We subsequently simulated the Bayesian sensory integration model with both the traditional Gaussian distribution prior and with the best-fit t Location-Scale distribution prior. For the other sensory parameters (see Table 5), we used the best-fit parameters obtained in previous studies (Alberts et al., 2016; Clemens et al., 2011). Thus, only the parameters relating to the prior differed between individuals, while the other parameters were kept constant across participants. Figure 6 shows the expected systematic error in the head-in-space estimate as a function of head roll-tilt, ranging from -120 degrees (CCW) to +120 degrees (CW).

Gaussian Prior

With the Gaussian prior, the systematic errors simulated by the model closely correspond to previous findings of systematic errors on SVV tasks (e.g. Alberts et al., 2016; Clemens et al., 2011; De Vrijer et al., 2008). At the maximum head-tilt of 120 degrees the systematic errors ranged between roughly 50° (S1) and 76° (S4). Thus, when being roll-tilted 120°, a presented line would need to be rotated between 50° to 76° in the head-tilt direction to be perceived as completely vertical, because the participants severely underestimate their own head-tilt. These large individual differences are caused by the different variances of the priors. As is shown in Table 4, S1 and S4 have the largest and smallest variances of the fitted Gaussian prior, respectively (S1: *SD* = 9.59; S4: *SD* = 6.17). Because the prior is

Table 3. AIC scores of t location-scale fits and Gaussian fits. *Note.* The smaller the score, the better the fit. A difference in scores of >10 is considered significant.

Subject	t Location-Scale	Gaussian
S1	884707.32	898018.93
S2	746903.99	753097.96
S3	864914.41	875360.34
S4	738085.19	749794.17
S5	699767.01	723877.08
S6	908216.10	917149.47

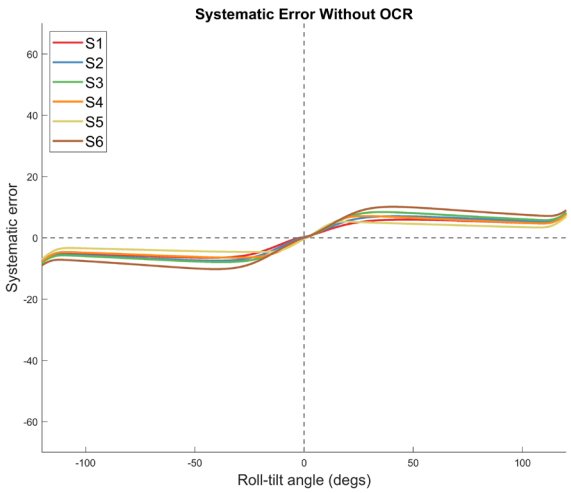

Figure 8. Simulated systematic errors without uncompensated ocular counterroll with t location-scale prior. *Note.* S = Subject; OCR = Ocular counterroll.

weighted according to its variance in the integration stage of the model, the prior is weighted less in S1 and weighted more in S4, resulting in the simulated differences in systematic errors. At small roll-tilt angles, however, the E-effect becomes visible, where small systematic errors in the *opposite* direction of the head-tilt appear, as if the brain overestimates one's own head-tilt. This is caused by the aforementioned uncompensated ocular counterroll (, in the model). Figure 7 shows the variance of the resulting head-in-space estimate as a function of head-tilt. Again, S1 shows the largest variance in the head-in-space estimate at large tilt-angles, which is explained by the high-variance prior. Regarding the magnitudes of the variances, they also correspond to the equivalent values reported in previous studies. Near upright, the smaller variances of the final estimate indicate lower uncertainty. As roll-tilt increases, so does the uncertainty in the head-in-space estimate. Thus, simulating the Bayesian optimal integration model by using the Gaussian distributions that were obtained from the naturalistic head orientation distributions resulted in systematic errors and head-in-space estimate variances that closely correspond to previously reported results on tasks of perceived verticality.

Table 4. Parameters of the Gaussian prior and the t location-scale prior. *Note.* Note that the μ and the σ do not correspond to the same thing in the Gaussian and t Location-Scale case. In the latter case, μ = location parameter and σ = scale parameter, not Mean and SD.

Subject	Gaussian prior		t Location-Scale prior		
	μ	σ	μ	σ	ν
S1	-2.62	9.59	-1.92	6.92	3.87
S2	-1.98	7.59	-0.94	5.82	4.42
S3	0.48	6.44	0.91	4.98	4.79
S4	0.82	6.17	1.10	4.41	3.71
S5	1.16	6.98	1.05	3.97	2.37
S6	-0.08	6.26	-0.10	5.13	6.19

t Location-Scale prior

For the t Location-Scale distribution prior, this was not the case. Although providing a much better fit to the naturalistic data, the simulated systematic errors do not correspond to both the Gaussian prior version of the simulation and previously measured systematic errors on SVV tasks. In contrast to what would be expected, the systematic errors are 1) much smaller in magnitude (ranging between 6.83° (S6) and 11.06° (S5)) and 2) in the opposite direction of what previous studies have reported. Furthermore, differences between individuals are rather small and do not correspond to the individual differences from the simulation with the Gaussian prior (i.e. S6 and S5 with minimum and maximum systematic errors, compared to S1 and S4 in the Gaussian prior simulation). In contrast to the systematic error, the variance of the final head-in-space estimate corresponds more closely to the variance profile of the Gaussian prior simulation, with higher variances at large head-tilts, compared to upright. However, at head-tilt angles beyond 100°, the variance suddenly decreases significantly, as if uncertainty about one's own head-tilt also decreases. Thus, even though the t Location-Scale distribution fits the naturalistic head-orientation data considerably better than a Gaussian distribution, it does not seem to be able to capture the previously observed systematic errors and variances in the final head-in-space estimate.

Table 5. Best-fit parameter values adapted from previous studies. *Note.* α_{HS} = proportional variance increase of otolith signal; β_{HS} = base signal; σ^2_{BS} = variance body-in-space signal; σ^2_{HR} = variance head-on-body signal; A_{OCR} = uncompensated ocular counterroll.

Parameters	α_{HS}	β_{HS}	σ^2_{BS}	σ^2_{HR}	A_{OCR}
Values	0.16	2.4	10.8	4.9	14.6

Discussion

This study investigated whether motion tracking of naturalistic activities can serve as a viable methodological approach to represent and model the underlying head-in-space prior as part of a Bayesian multisensory integration framework. More specifically, we investigated what type of distribution best fits the real-world head orientation data and whether it can be successfully integrated in the Bayesian optimal integration model to explain performances on tasks of perceived verticality. Based on the assumptions from previous research (e.g. Alberts et al., 2016; Clemens et al., 2011; De Vrijer et al., 2008; MacNeilage et al., 2007)2007, we assumed the naturalistic head orientation distributions to be best described by Gaussian distributions and that we would be able to adequately simulate what the SVV task performance would look like in these subjects. The hypotheses were not supported. We showed that a Gaussian distribution is not able to capture the peaks and tails of the naturalistic head orientation distributions. In fact, the best fit was provided by the tLocation-Scale distributions. However, upon simulating the Bayesian optimal integration model with both the best-fitting Gaussian distribution and the t Location-Scale distribution as the prior, only the Gaussian prior version of the model simulated the biases that were observed in previous studies of verticality perception in a realistic way.

Why the simulated SVV task performances do not correspond to previous findings

Two reasons contribute to the finding that the systematic errors that resulted from the model simulation incorporating the t Location-Scale prior did not correspond to previous findings on tasks of verticality perception. Figure 8 illustrates, what the systematic error would look like if the uncompensated ocular counterroll was *not* added to the final estimate (Equation 16). It becomes clear that in that case, the errors go in the direction of the head-tilt, which is in line with previous research, but they only reach values of about 10°, therefore being far smaller than what was expected. Prior research has shown that systematic errors can reach magnitudes up to 60° at head-tilts of 120° (Clemens et al., 2011). The small magnitude of the systematic error observed here is partly caused by the fat tails of the t Location-Scale prior. The effect this has on the model simulation is remarkable. Even though the t Location-Scale distributions appear to be smaller in width than the normal distributions, they have far fatter tails. This causes the prior to be weighted less in the signal integration stage of the model. Thus, it only slightly pulls the final head-in-space estimate towards zero, resulting in a much smaller systematic error.

If then, on top of the already small systematic errors, the OCR is added to the error, this results in the observed systematic errors of the model simulation. As can be inferred from Equation 15, the OCR is essentially represented as a relatively large sinusoid that is added on top of the head-in-space error, causing the systematic error to go in the direction opposite of the actual head-tilt. Thus, both the fat tails of the t Location-Scale prior and the OCR that is added on top of the error cause the model simulation to inaccurately predict the SVV task performance.

Can the model work with t Location-Scale priors?

How could the simulation of the SVV task performance be improved in the case of the t Location-Scale prior? One of the main limitations of the present study is that the variances of the various sensory signals were fixed in the model simulation. This is problematic, because the variances were adapted from previous research under the assumption that the prior is of Gaussian nature. Replacing the Gaussian prior for a t Location-Scale prior, while keeping the variances of the sensory signals fixed, thus causes the presented results. To compensate for the different properties of the t Location-Scale distribution (e.g. the fatter tails), the variances of the sensory signals would need to be adjusted, too. This could be achieved by either increasing the variances of the otolith signal and the indirect body signal, therefore increasing the relative weight of the t Location-Scale prior, and/or by reducing the large effect that the uncompensated ocular counterroll has on the results. Ideally, this would be achieved by letting the same participants that took part in the motion tracking experiment perform an SVV task. One could then fit the Bayesian multisensory integration model to the SVV data. In that case, the prior would be fixed, because it is based on the previously measured head orientation distributions, while the sensory signals are fitted to the data as free parameters. This should provide a more accurate fit of the model and, in turn, should result in more realistic parameters for the various signals that are

part of the multisensory integration model. Due to the current situation regarding the COVID-19 crisis, such an experiment was unfortunately not possible, but should be considered in future research.

Implications for future research

In the current study, we were able to extensively quantify head orientations during everyday life activities. We demonstrated that wireless motion tracking can be flexibly used to accurately quantify everyday life activities and that it can serve as a way to combine naturalistic tasks with controlled lab-based measures to investigate spatial orientation. Using a similar naturalistic approach, Carriot and colleagues (2014) have shown that the vestibular system has to deal with angular velocities that deviate considerably from normality. Here we showed that the same applies to probability distributions of head-orientations in the roll-tilt dimension. Participants' head orientation distributions were all roughly centered on upright and, apart from one subject, largely non-skewed. However, the probability distributions were characterized by fatter tails, as indicated by higher kurtoses. Thus, in everyday life, participants experience more extreme head-tilts in the roll dimension than what a normal distribution is able to capture. Assuming that the underlying head-in-space prior is based on lifelong experiences of how the head is typically oriented in space, and further assuming that the activities used in the current study are a realistic representation of everyday life activities, it can be concluded that the underlying prior deviates considerably from normality. Thus, frequently observed individual differences on SVV tasks could be explained by different underlying priors, and, therefore, different naturalistic head orientation distributions. Future research should explore this possibility more extensively.

In the current study, we have challenged the assumption that the head-in-space prior is of Gaussian nature. Apart from the head-in-space prior, the original model (Clemens et al., 2011) also assumed the sensory information from the various sources (otoliths, neck, body somatosensors) to be corrupted by Gaussian noise. Therefore, the question can be asked whether the sensory information from those sources is also non-Gaussian, contrary to what is assumed in the multisensory integration model. Future research could look into the specific statistical characteristics of the different sensory signals. It should be noted though that we would not expect the multisensory integration model to predict significantly different results, even if the sensory signals are found to be of non-Gaussian nature, too. This is because the sensory signals are assumed to be unbiased and, thus, to be centered on the true head/body tilt, while the systematic errors that the model predicts are solely elicited by the prior. The specific shape of the distributions of the sensory signals would therefore not have a large impact on the multisensory integration process. An alternative multisensory integration model that employs unbiased, albeit non-Gaussian sensory signals, would likely predict very similar systematic errors in the head-in-space estimate compared to the original model.

We assumed the line-relative-to-eye information (i.e. the sensory information of how the line falls onto the retina) to be unbiased. However, Girshick, Landy and Simoncelli (2011) have shown that observers are biased towards perceiving cardinal (i.e. horizontal, vertical) relative to oblique orientations. They argue that these biases might occur due to a prior centered on the two cardinal orientations (i.e. 0° and 90°). Thus, in addition to the head-in-space prior that is solely centered on upright, future work might include an additional "line-relative-to-eye prior" that is centered on 0° and 90° and could therefore account for the biases found by Girshick et al. (2011). In the present study, we chose to use an unbiased line-relative-to-eye representation so that we employ a multisensory integration model that only differs from previous studies in its head-in-space prior, while keeping all other components of the model the same. This made comparisons with previous findings (e.g. Clemens et al. (2011)) substantially easier.

Future projects should also consider the possibility of applying the current approach to patient groups with vestibular disorders, potentially providing novel evidence about the underlying priors in such populations. Previous research has shown that patients with bilateral vestibular function loss tend to show a larger bias in the SVV task at large head-tilts (90°) compared to control subjects (Alberts et al., 2015). In line with the Bayesian optimal integration model (Clemens et al., 2011), this can theoretically be explained by the fact that the brain in those patient groups is not able to use vestibular information. Instead, contributions from other sensory signals regarding head-in-space orientation and the contribution from the prior will be weighted more heavily, resulting in larger systematic errors. Investigating how these patients orient their heads during naturalistic activities and what that indicates with regards to the underlying prior might, therefore, provide valuable evidence

regarding the underlying mechanisms taking place to achieve spatial orientation in patients with vestibular function loss.

Limitations

One of the limitations of the current study is the fact that the chosen naturalistic activities constrain the head movements of the participants, in that it is advantageous to keep the head as stable as possible to maintain spatial orientation, for example during the running task. This leads to relatively small inter-subject differences in both the head orientation distributions and, after integration of those distributions in the model, SVV task performance simulations. In future research it could be considered to introduce activities that force participants to move their heads around more extensively. Even if those activities would not perfectly represent the activities that the underlying prior is based on, they would allow for larger inter-subject differences, which, in turn, might be correlated to inter-subject differences on SVV task performance, providing evidence that everyday life head movements might influence lab-based tasks of verticality perception.

Conclusion

Here we were able to, for the first time, measure and quantify head orientations during naturalistic activities, providing novel evidence of what the underlying head-in-space prior as part of a Bayesian multisensory integration model might look like. In contrast to how the prior has been modelled in previous studies, we showed that head orientation distributions deviate from normality and are characterized by fatter tails, indicating that the underlying head-in-space prior might, too, be of non-Gaussian nature. T Location-Scale distributions provided the best fit to the data in the vast majority of the subjects. However, after integrating those distributions as representations of the prior in the model, simulations of SVV task performance did not correspond to previous behavior on tasks of verticality perception regarding both the direction and magnitude of the systematic errors. This was caused by the properties of the t Location-Scale distribution (i.e. the fat tails) and the fact that the variances of the sensory signals were not adjusted to account for those specific properties of the prior. Future research should investigate this more extensively, for example by adjusting the motion tracked real-world activities to elicit more inter-subject differences in head orientations. Those same subjects would subsequently participate in a task on verticality perception to investigate correlations between individual differences of naturalistic head orientation distributions and lab-based tasks of perceived verticality.

References

Alberts, B. B. G. T., Selen, L. P. J., Bertolini, G., Straumann, D., Medendorp, W. P., &Tarnutzer, A. A. (2016). Dissociating vestibular and somatosensory contributions to spatial orientation. *Journal of Neurophysiology*, *116*(1), 30–40. https://doi.org/10.1152/jn.00056.2016

Alberts, B. B. G. T., Selen, L. P. J., Verhagen, W. I. M., &Medendorp, W. P. (2015). Sensory substitution in bilateral vestibular a-reflexic patients. *Physiological Reports*, *3*(5), e12385. https://doi.org/10.14814/phy2.12385

Aubert, H. (1861). Eine scheinbare bedeutende Drehung von Objecten bei Neigung des Kopfes nach rechts oder links. *Archiv für pathologische Anatomie und Physiologie und für klinische Medicin*, *20*(3), 381–393. https://doi.org/10.1007/BF02355256

Barra, J., Marquer, A., Joassin, R., Reymond, C., Metge, L., Chauvineau, V., &Pérennou, D. (2010). Humans use internal models to construct and update a sense of verticality. *Brain*, *133*(12), 3552–3563. https://doi.org/10.1093/brain/awq311

Breckenridge, W. G. (1979). *Quaternions proposed standard conventions* [Technical Report]. NASA Jet Propulsion Laboratory.

Brown, S. (2016). *Measures of Shape: Skewness and Kurtosis*. https://brownmath.com/stat/shape.htm#Kurtosis

Burnham, K. P., & Anderson, D. R. (2002). *Model Selection and Multimodel Inference: A Practical Information-Theoretic Approach* (2nd ed.). Springer-Verlag. https://doi.org/10.1007/b97636

Carriot, J., Jamali, M., Chacron, M. J., & Cullen, K. E. (2014). Statistics of the vestibular input experienced during natural self-motion: Implications for neural processing. *The Journal of Neuroscience: The Official Journal of the Society for Neuroscience*, *34*(24), 8347–8357. https://doi.org/10.1523/JNEUROSCI.0692-14.2014

Cavanaugh, J. E., & Neath, A. A. (2019). The Akaike information criterion: Background, derivation, properties, application, interpretation, and refinements. *WIREs Computational Statistics*, *11*(3), e1460. https://doi.org/10.1002/wics.1460

Ceyte, H., Cian, C., Trousselard, M., & Barraud, P.-A. (2009). Influence of perceived egocentric coordinates on the subjective visual vertical. *Neuroscience Letters*, *462*(1), 85–88. https://doi.org/10.1016/j.neulet.2009.06.048

Clemens, I. A. H., De Vrijer, M., Selen, L. P. J., Van Gisbergen, J. A. M., & Medendorp, W. P. (2011). Multisensory processing in spatial orientation: An inverse probabilistic approach. *The Journal*

of Neuroscience: The Official Journal of the Society for Neuroscience, *31*(14), 5365–5377. https://doi.org/10.1523/JNEUROSCI.6472-10.2011

De Castro, F. (2020). *Fitmethis*. MATLAB Central File Exchange. https://de.mathworks.com/matlabcentral/fileexchange/40167-fitmethis

De Vrijer, M., Medendorp, W. P., &Gisbergen, J. A. M. V. (2009). Accuracy-precision trade-off in visual orientation constancy. *Journal of Vision*, *9*(2), 9–9. https://doi.org/10.1167/9.2.9

De Vrijer, M., Medendorp, W. P., & Van Gisbergen, J. a. M. (2008). Shared computational mechanism for tilt compensation accounts for biased verticality percepts in motion and pattern vision. *Journal ofNeurophysiology*, *99*(2), 915–930. https://doi.org/10.1152/jn.00921.2007

De Winkel, K. N., Katliar, M., Diers, D., &Bülthoff, H. H. (2018). Causal Inference in the Perception of Verticality. *Scientific Reports*, *8*(1), 5483. https://doi.org/10.1038/s41598-018-23838-w

Dieterich, M., & Brandt, T. (2019). Perception of Verticality and Vestibular Disorders of Balance and Falls. *Frontiers in Neurology*, *10*. https://doi.org/10.3389/fneur.2019.00172

Eggert, T. (1998). *Der Einfluss orientierter Texturen auf die subjektive visuelle Vertikale und seine systemtheoretische Analyse* [PhD thesis]. Technical University of Munich.

Girshick, A. R., Landy, M. S., &Simoncelli, E. P. (2011). Cardinal rules: Visual orientation perception reflects knowledge of environmental statistics. *Nature Neuroscience*, *14*(7), 926–932. https://doi.org/10.1038/nn.2831

Hemingway, E. G., & O'Reilly, O. M. (2018). Perspectives on Euler angle singularities, gimbal lock, and the orthogonality of applied forces and applied moments. *Multibody System Dynamics*, *44*(1), 31–56. https://doi.org/10.1007/s11044-018-9620-0

Körding, K. P., & Wolpert, D. M. (2004). Bayesian integration in sensorimotor learning. *Nature*, *427*(6971), 244. https://doi.org/10.1038/nature02169

MacNeilage, P. R., Banks, M. S., Berger, D. R., &Bülthoff, H. H. (2007). A Bayesian model of the disambiguation of gravitoinertial force by visual cues. *Experimental Brain Research*, *179*(2), 263–290. https://doi.org/10.1007/s00221-006-0792-0

MacNeilage, P. R., Ganesan, N., &Angelaki, D. E. (2008). Computational approaches to spatial orientation: From transfer functions to dynamic bayesian inference. *Journal of Neurophysiology*, *100*(6), 2981–2996. https://doi.org/10.1152/jn.90677.2008

MathWorks—Normal Distribution. (2020). Normal Distribution. https://de.mathworks.com/help/stats/normal-distribution.html

Mittelstaedt, H. (1983). A new solution to the problem of the subjective vertical. *Naturwissenschaften*, *70*(6), 272–281. https://doi.org/10.1007/BF00404833

Murray, R. F., & Morgenstern, Y. (2010). Cue combination on the circle and the sphere. *Journal of Vision*, *10*(11), 15–15. https://doi.org/10.1167/10.11.15

Normality Testing—Skewness and Kurtosis. (n.d.). GoodData Documentation. Retrieved 4 July 2020, from https://help.gooddata.com/doc/en/reporting-and-dashboards/maql-analytical-query-language/maql-expression-reference/aggregation-functions/statistical-functions/predictive-statistical-use-cases/normality-testing-skewness-and-kurtosis#:~:text=As%20a%20general%20rule%20of,the%20distribution%20is%20approximately%20symmetric.

Palla, A., Bockisch, C. J., Bergamin, O., & Straumann, D. (2006). Dissociated hysteresis of static ocular counterroll in humans. *Journal of Neurophysiology*, *95*(4), 2222–2232. https://doi.org/10.1152/jn.01014.2005

Rosenthal, R. (1994). Parametric measures of effect size. In H. Cooper & L. V. Hedges (Eds.), *The handbook of research synthesis* (pp. 231–244). Russell Sage Foundation.

Stocker, A. A., &Simoncelli, E. P. (2006). Noise characteristics and prior expectations in human visual speed perception. *Nature Neuroscience*, *9*(4), 578–585. https://doi.org/10.1038/nn1669

Tarnutzer, A. A., Bockisch, C. J., & Straumann, D. (2010). Roll-dependent modulation of the subjective visual vertical: Contributions of head- and trunk-based signals. *Journal of Neurophysiology*, *103*(2), 934–941. https://doi.org/10.1152/jn.00407.2009

Tarnutzer, A. A., Bockisch, C., Straumann, D., &Olasagasti, I. (2009). Gravity dependence of subjective visual vertical variability. *Journal of Neurophysiology*, *102*(3), 1657–1671. https://doi.org/10.1152/jn.00007.2008

Van Beuzekom, A. D., & Van Gisbergen, J. A. (2000). Properties of the internal representation of gravity inferred from spatial-direction and body-tilt estimates. *Journal of Neurophysiology*, *84*(1), 11–27. https://doi.org/10.1152/jn.2000.84.1.11/F

Xsens. (2017). *MVN Analyze*. https://www.xsens.com/products/mvn-analyze

Appendix

Table 6. All fitted distributions and their respective parameters.

Distribution type	Parameter 1	Parameter 2	Parameter 3
Normal Distribution	μ: mean	σ: standard deviation	-
Exponential Distribution	μ: mean	-	-
Gamma Distribution	a: shape parameter	b: scale parameter	-
Logistic Distribution	μ: mean	σ: scale parameter	-
t Location-Scale Distribution	μ: location parameter	σ: scale parameter	ν: shape parameter
Uniform Distribution	a: lower endpoint (minimum)	b: upper endpoint (maximum)	-
Extreme Value Distribution	μ: location parameter	σ: scale parameter	-
Rayleigh Distribution	b: scale parameter	-	-
Generalized Extreme Value Distribution	k: shape parameter	σ: scale parameter	μ: location parameter
Beta Distribution	a: first shape parameter	b: second shape parameter	-
Nakagami Distribution	μ: shape parameter	ω: scale parameter	-
Rician Distribution	s: noncentrality parameter	σ: scale parameter	-
Inverse Gaussian Distribution	μ: scale parameter	λ: shape parameter	-
Birnbaum-Saunders Distribution	β: scale parameter	γ: shape parameter	-
Generalized Pareto Distribution	k: tail index parameter	σ: scale parameter	θ: threshold parameter
Loglogistic Distribution	μ: mean of logarithmic values	σ: scale parameter of logarithmic values	-
Lognormal Distribution	μ: mean of logarithmic values	σ: scale parameter of logarithmic values	-
Weibull Distribution	a: scale parameter	b: shape parameter	-